Acta Cryst. (1983). B39, 657–663

Neutron Structural Study of the Successive Phase Transitions in Rb_2ZnCl_4

BY M. QUILICHINI† AND J. PANNETIER

Institut Laue–Langevin, 156X Centre de Tri, 38042 Grenoble CEDEX, France

(*Received* 13 *December* 1982; *accepted* 8 *March* 1983)

Abstract

The crystal structures of Rb_2ZnCl_4 at 300, 235, 100 and 60 K were investigated from neutron single-crystal diffraction data. Refinements in space groups *Pnma* ($Z = 4$, average structure of the incommensurate phase at 300 and 235 K) and $Pna2_1$ ($Z = 12$, 100 and 60 K) converged to R values of 0·084, 0·085, 0·046 and 0·025, respectively. The strong anisotropy of the thermal parameters of chlorine atoms at 300 and 235 K suggests the presence of a static modulated distortion in the incommensurate phase. However, this displacive model is not sufficient to account for the successive phase transitions. Evidence is given that the $ZnCl_4$ group undergoes a large libration motion. The orientation of each group derives from its position in the paraelectric phase ($T > 302$ K) by a rotation around the pseudo-hexagonal axis a which is the direction of tripling of the ferroelectric-phase unit cell ($T < 189$ K). The structure of this ferroelectric phase is given. At 60 K a space group is proposed for the low-temperature phase ($T < 74$ K) based both on an analysis of the experimental data and on group-theory considerations. The present structural results are compared with those obtained by NMR and NQR spectroscopy.

I. Introduction

In the present paper we report neutron structural measurements on Rb_2ZnCl_4 known to exhibit successive phase transitions similar to those of other A_2BX_4 materials whose prototype is K_2SeO_4.

In Rb_2ZnCl_4 the observed phases are (Table 1): phase II ($T > T_I = 302$ K) which is paraelectric and whose space group *Pnma* is derived from the hexagonal $P6_3/mma$ of phase I; phase III ($T_c = 189$ K $< T < 302$ K) is incommensurate with a modulation $\mathbf{q}_0 = (\mathbf{a}^*/3)[1 - \delta(T)]$; phase IV ($T_0 = 74$ K $< T < 189$ K) is ferroelectric $Pna2_1$ with a spontaneous polarization along the b axis of the paraelectric phase and a unit cell tripled along the pseudo-hexagonal axis a of *Pnma*; phase V ($T < T_0$) is suggested by many techniques (Raman, optical) (Francke, Le Postollec, Mathieu & Poulet, 1980; Unruh & Strömich, 1981; Günter, Sanctuary & Rohner, 1982) and is also known to be ferroelectric. It has been shown (Unruh & Strömich, 1981) that in phase V a spontaneous polarization $\mathbf{P}_a$ parallel to the pseudo-hexagonal a axis appears at $T = T_0$ and increases as T decreases while the spontaneous polarization $\mathbf{P}_b$ of the ferroelectric phase decreases with decreasing T. Furthermore, the behaviour of the relative permittivity $\mathbf{K}_a$ at T_0 resembles that of a purely structural transition of second order and the high index of faintness n (=4 or 6) suggests the formation of an improper ferroelectric.

In order to explain the mechanism of the successive phase transitions in Rb_2ZnCl_4, it is necessary to make detailed studies on the crystal structures of all phases.

The format of this paper is as follows. We first give a brief description of the experimental procedures in § II; in § III we describe the average structure of the incommensurate phase at two temperatures (300 and 235 K), the precise determination of ferroelectric phase IV, the refinement of the structure of phase V using the space group of phase IV; in § IV we shall discuss the structural modulation involved in these transitions; in § V, using the results of § III, we shall give our conclusion as to the space group of phase V.

II. Experimental

Single crystals of Rb_2ZnCl_4 were grown from aqueous solution by slow evaporation. The single crystal used for these experiments has natural faces {301}, {011},

Table 1. *Crystal data of* Rb_2ZnCl_4 *at* 300, 235, 100 *and* 60 K

T (K)	60	100	235	300
Space group	$Pna2_1$	$Pna2_1$	*Pnma**	*Pnma*
Formula units per unit cell (Å)	12	12	4	4
a (Å)	27·439 (9)	27·505 (9)	9·218 (9)	9·233 (4)
b (Å)	12·542 (4)	12·627 (6)	7·275 (6)	7·278 (5)
c (Å)	7·201 (3)	7·242 (3)	12·722 (8)	12·736 (8)

* Average symmetry of the incommensurate phase.

† DRP, Université Pierre et Marie Curie, 4 place Jussieu, 75230 Paris CEDEX 05, France.

0108-7681/83/060657-07$01.50

{001}. The size was about 3·6 × 2·3 × 1 mm. Neutron single-crystal experiments were performed at 300, 235, 100 and 60 K on the D9 four-circle diffractometer located on the hot source of the ILL. Data were collected with a wavelength of 0·841 Å. The crystal was mounted in a Displex® cryostat which allows the temperature fluctuations to be kept within ±0·5 K.

Totals of 808 (RT), 704 (235 K), 2283 (100 K) and 2394 (60 K) reflections with $0 < h, l < 32$ were measured by ω scans to $\sin\theta/\lambda = 0{\cdot}682$ Å^{-1}. The raw data were reduced to F^2 values by the method of Lehmann & Larsen (1979). The data were corrected for absorption ($\mu = 1{\cdot}4$ cm^{-1}) using the method of Coppens & Hamilton (1970). The data were then averaged so that the final refinements in space group *Pnma* are based on 786 independent reflections with $F/\sigma(F) > 2$ at 300 K, and on 684 independent reflections at 235 K. The refinements in space group $Pna2_1$ are based on 2186 and 1854 independent reflections at 100 and 60 K, respectively. The scattering lengths were taken from Koester & Rauch (1979): b(Rb) = 7·08, b(Zn) = 5·68, b(Cl) = 9·58 fm.

Refinement calculations were performed using the program *SHELX* (Sheldrick, 1976). A Fortran thermal-ellipsoid-plot program has been used for crystal structure illustrations (*ORTEP*, Johnson, 1965).

III. Results

III.1. *Structure refinements*

At 300 and 235 K the crystal is in the incommensurate phase. The least-squares calculations were performed in the paraelectric centrosymmetric space group *Pnma* which is the 'average' structure of the incommensurate phase.

Table 2(*a*,*b*,*c*)* gives the results of structure refinements at 300 and 235 K under the conditions defined in § II. Refinement with anisotropic thermal parameters converged to $R = \sum(|F_o| - |F_c|)/\sum|F_o| = 0{\cdot}0882$; $R_w = \sum w^{1/2}|F_o - F_c|/\sum w^{1/2}|F_o| = 0{\cdot}1077$ for 300 K ($w = 1/\sigma^2$) and to $R = 0{\cdot}0882$, $R_w = 0{\cdot}1098$ for 235 K.*

The presence of the static modulated distortion is suggested by the observation of anomalously large thermal parameters. For example, at 300 K U_{22} is 0·1389 and 0·1572 Å^2 for Cl(1) and Cl(2) respectively and U_{33} is 0·1162 Å^2 for Cl(3).

* Lists of observed and calculated structure factors at 300, 235, 100 and 60 K, anisotropic thermal parameters and parts *c* and *f* of Table 2 have been deposited with the British Library Lending Division as Supplementary Publication No. SUP 38486 (47 pp.). Copies may be obtained through The Executive Secretary, International Union of Crystallography, 5 Abbey Square, Chester CH1 2HU, England.

Table 2. *Atomic fractional coordinates* (×10^4) *and thermal parameters* (*see deposition footnote*) *for* Rb_2ZnCl_4

E.s.d.'s are in parentheses and refer to the last digit. Asterisks indicate fixed values.

$$B_{eq} = \tfrac{8}{3}\pi^2 \sum_i \sum_j U_{ij} a_i^* a_j^* \mathbf{a}_i \cdot \mathbf{a}_j.$$

	x	y	z	B_{eq} (Å^2)
(*a*) *Pnma*, 300 K				
Rb(1)	6314 (3)	¼*	4075 (3)	2·81 (1)
Rb(2)	4851 (2)	¼*	8196 (2)	1·73
Zn(1)	2246 (3)	¼*	4225 (2)	1·10
Cl(1)	9839 (2)	¼*	4173 (2)	3·01 (1)
Cl(2)	3185 (2)	¼*	5854 (2)	3·18 (1)
Cl(3)	3159 (2)	10007 (2)	3425 (2)	3·30
(*b*) *Pnma*, 235 K				
Rb(1)	6298 (4)	¼*	4067 (4)	2·43 (1)
Rb(2)	4862 (3)	¼*	8196 (2)	1·42 (1)
Zn(1)	2240 (3)	¼*	4217 (2)	0·87 (1)
Cl(1)	9825 (3)	¼*	4189 (2)	2·84 (1)
Cl(2)	3204 (3)	¼*	5851 (2)	3·31 (1)
Cl(3)	3139 (3)	10010 (3)	3410 (3)	3·51 (1)
(*d*) $Pna2_1$, 100 K				
Rb(1)	2089 (1)	4047 (3)	2424 (5)	1·21 (1)
Rb(2)	424 (1)	900 (2)	2804 (5)	1·12 (1)
Rb(3)	3769 (1)	987 (3)	2639 (5)	1·30 (1)
Rb(4)	1631 (1)	8189 (2)	2452 (5)	0·80 (1)
Rb(5)	3292 (1)	6807 (2)	2498 (5)	0·79 (1)
Rb(6)	4960 (1)	8182 (2)	2805 (5)	0·75 (1)
Zn(1)	735 (1)	4222 (2)	¼*	0·57 (1)
Zn(2)	2414 (1)	792 (2)	2551 (4)	0·60 (1)
Zn(3)	4072 (1)	4208 (2)	2706 (4)	0·61 (1)
Cl(1)	1604 (1)	795 (2)	2794 (5)	1·25 (1)
Cl(2)	3261 (1)	4199 (2)	2916 (5)	1·22 (1)
Cl(3)	4932 (1)	748 (1)	2058 (4)	0·92 (1)
Cl(4)	1084 (1)	5825 (1)	3010 (4)	0·94 (1)
Cl(5)	2754 (1)	9176 (2)	1993 (4)	0·95 (1)
Cl(6)	4408 (1)	5839 (2)	3029 (5)	1·16 (1)
Cl(7)	1101 (1)	3624 (2)	9859 (4)	0·94 (1)
Cl(8)	2656 (1)	1918 (2)	308 (4)	1·16 (1)
Cl(9)	4351 (1)	3562 (2)	9999 (4)	1·22 (1)
Cl(10)	616 (1)	8168 (2)	9954 (4)	1·32 (1)
Cl(11)	2250 (1)	6346 (1)	245 (4)	0·91 (1)
Cl(12)	4050 (1)	8127 (2)	9812 (4)	1·13 (1)
(*e*) $Pna2_1$, 60 K				
Rb(1)	2085 (1)	4041 (3)	2422 (5)	0·87 (1)
Rb(2)	423 (1)	910 (2)	2802 (5)	0·86 (1)
Rb(3)	3769 (1)	978 (3)	2640 (5)	0·97 (1)
Rb(4)	1637 (1)	8191 (2)	2418 (5)	0·64 (1)
Rb(5)	3292 (1)	6809 (2)	2483 (4)	0·48 (1)
Rb(6)	4961 (1)	8177 (2)	2820 (5)	0·41 (1)
Zn(1)	735 (1)	4219 (2)	¼*	0·32 (1)
Zn(2)	2415 (1)	794 (2)	2538 (3)	0·36 (1)
Zn(3)	4068 (1)	4208 (2)	2696 (3)	0·31 (1)
Cl(1)	1603 (1)	800 (2)	2801 (4)	0·75 (1)
Cl(2)	3257 (1)	4203 (2)	2932 (4)	0·84 (1)
Cl(3)	4929 (1)	724 (1)	2015 (4)	0·48 (1)
Cl(4)	1089 (1)	5821 (1)	3032 (4)	0·69 (1)
Cl(5)	2755 (1)	9185 (2)	1973 (4)	0·80 (1)
Cl(6)	4411 (1)	5824 (1)	3075 (4)	0·89 (1)
Cl(7)	1100 (1)	3623 (1)	9861 (4)	0·64 (1)
Cl(8)	2652 (1)	1934 (1)	308 (4)	0·85 (1)
Cl(9)	4344 (1)	3581 (1)	9970 (4)	0·95 (1)
Cl(10)	620 (1)	8125 (1)	9909 (4)	0·86 (1)
Cl(11)	2249 (1)	6341 (1)	249 (4)	0·62 (1)
Cl(12)	4061 (1)	8113 (1)	9812 (4)	0·72 (1)

At 100 K the crystal is in the ferroelectric phase (space group $Pna2_1$). The spontaneous polarization is along the **c** axis of this group. The unit cell of this phase is tripled along the pseudo-hexagonal axis with respect to the unit cell of the paraelectric phase (*Pnma*). The refinement with anisotropic thermal parameters gives $R = 0{\cdot}0465$, $R_w = 0{\cdot}0493$.

At 60 K the crystal is known to be in phase V. Structure refinements were performed using the ferroelectric space group $Pna2_1$. They converge to $R = 0{\cdot}0266$, $R_w = 0{\cdot}0253$. Nevertheless, one must notice that this space group is not correct because some Bragg reflections forbidden in space group $Pna2_1$ are observed.

This confirms our previous powder data (Pannetier & Quilichini, 1980). It must also be mentioned that all these Bragg peaks are weak and even though the structural phase transition IV–V is unquestionable, it certainly involves a subtle atomic-position rearrangement.

III.2. *Thermal parameters*

Anisotropic thermal parameters (deposited) suggest that the $ZnCl_4$ group undergoes a large librational motion. Following the treatment by Cruickshank (1956) as extended by Schomaker & Trueblood (1968) the anisotropic rigid-body translational and librational tensors were calculated for the $ZnCl_4$ groups at each temperature (300, 235, 100 and 60 K).

In Table 2(*c*, *f*) (deposited) we give the r.m.s. translation along the axes of the crystal. The Zn–Cl bond lengths corrected for the libration motion are given in Tables 3 and 4. The details of the rigid-body calculations for 300 K (**T**, **L**, **S** matrices for each $ZnCl_4$ group) are presented in Table 5. Fig. 1 shows *ORTEP* projections of the structure on one principal plane at 300 and 100 K.

In Fig. 2 it is clearly seen that the orientation of each $ZnCl_4$ group in the phase at 100 K is derived from that at 300 K by a rotation around an axis nearly parallel to **a**. This rotation corresponds to the largest librational motion of the $ZnCl_4$ group at 300 K. At 100 K we also notice, amongst the three non-equivalent $ZnCl_4$ groups, that the shortest Zn–Cl bond is along **a** and slightly tilted with respect to **c**.

Table 3. *$ZnCl_4$-group correlation on going from the Pnma paraelectric phase to the $Pna2_1$ ferroelectric phase*

Paraelectric phase, *Pnma*	Ferroelectric phase, $Pna2_1$		
Zn	Zn(1) (I)	Zn(2) (II)	Zn(3) (III)
Cl(1)	Cl(3)	Cl(1)	Cl(2)
Cl(2)	Cl(4)	Cl(5)	Cl(6)
Cl(3)	Cl(7)	Cl(8)	Cl(9)
Cl(3)	Cl(12)	Cl(11)	Cl(10)
Cl(1)–Zn–Cl(2)	Cl(3)–Zn(1)–Cl(4)	Cl(1)–Zn(2)–Cl(5)	Cl(2)–Zn(3)–Cl(6)
Cl(1)–Zn–Cl(3)	Cl(3)–Zn(1)–Cl(7)	Cl(1)–Zn(2)–Cl(8)	Cl(2)–Zn(3)–Cl(9)
	Cl(3)–Zn(1)–Cl(12)	Cl(1)–Zn(2)–Cl(1)	Cl(2)–Zn(3)–Cl(10)
Cl(2)–Zn–Cl(3)	Cl(4)–Zn(1)–Cl(7)	Cl(5)–Zn(2)–Cl(8)	Cl(6)–Zn(3)–Cl(9)
	Cl(4)–Zn(1)–Cl(12)	Cl(5)–Zn(2)–Cl(11)	Cl(6)–Zn(3)–Cl(10)

III.3. *Electric-field-gradient tensors*

From the structural results given in § III.1 it is possible to calculate the electric-field-gradient (EFG) tensors for a given distribution of charges on the three ionic species, namely Rb, Zn and Cl. This charge distribution must obviously satisfy the electroneutrality condition and we assumed a charge of +1 on both Rb ions; then we are left with only one parameter which characterizes the distribution of charges over the $(ZnCl_4)^{2-}$ group. All calculations of the EFG tensors (monopolar contribution only) have been performed by direct summation over homothetical volumes of the unit cell followed by a linear extrapolation to infinite boundary (Coogan, 1967).

Table 4. *The bond lengths* (Å) *and angles* (°) *of the $ZnCl_4$ groups*

The uncorrected and corrected bond lengths for the librational motion of the $ZnCl_4$ group are given in the first and second lines respectively.

	300 K	235 K	100 K			60 K		
			I	II	III	I	II	III
Zn–Cl(1)	2·226 (3)	2·226 (4)	2·239 (3)	2·241 (3)	2·243 (3)	2·241 (3)	2·238 (3)	2·232 (3)
	2·245	2·245	2·244	2·247	2·249	2·243	2·242	2·238
Zn–Cl(2)	2·250 (3)	2·261 (4)	2·270 (3)	2·281 (4)	2·269 (3)	2·285 (4)	2·279 (4)	2·271 (4)
	2·291	2·309	2·277	2·287	2·282	2·291	2·286	2·282
Zn–Cl(3)	2·244 (2)	2·241 (2)	2·290 (3)	2·258 (3)	2·258 (3)	2·290 (4)	2·265 (3)	2·262 (3)
	2·279	2·281	2·295	2·267	2·269	2·294	2·273	2·272
Zn–Cl(3)	2·244 (2)	2·241 (2)	2·250 (4)	2·269 (3)	2·261 (4)	2·257 (3)	2·218 (4)	2·279 (4)
	2·279	2·281	2·258	2·276	2·271	2·263	2·287	2·287
Cl(1)–Zn–Cl(2)	114·3 (1)	114·0 (2)	115·3 (1)	115·2 (1)	113·1 (1)	114·7 (1)	115·2 (1)	113·9 (1)
Cl(1)–Zn–Cl(3)	111·2 (1)	111·3 (1)	108·8 (1)	110·5 (1)	113·4 (1)	108·1 (1)	110·1 (1)	113·5 (1)
			112·2 (1)	109·8 (1)	109·1 (1)	112·4 (1)	109·1 (1)	108·6 (1)
Cl(2)–Zn–Cl(3)	105·9 (1)	106·0 (2)	104·1 (1)	108·3 (1)	106·1 (1)	104·4 (1)	108·9 (1)	106·5 (1)
			108·3 (1)	105·1 (1)	107·2 (1)	108·7 (1)	105·2 (1)	107·6 (1)
Mean Zn–Cl (uncorrected bond)	2·241	2·242	2·262	2·262	2·258	2·268	2·265	2·261

Table 5. **L, S, T** *matrices at* 300 K *from rigid-body calculations for* $ZnCl_4$ *groups*

Librational tensors and e.s.d.'s (orthogonal axes)

L (rad²)

0·027 (1)	−0·000 (2)	−0·009 (2)
	0·005 (1)	−0·000 (2)
		0·012 (1)

S (rad Å)

−0·000 (0)	−0·001 (1)	−0·000 (1)
−0·001 (1)	−0·000 (2)	−0·003 (2)
−0·000 (2)	−0·002 (2)	0·000 (2)

T (Å²)

3·013 (2)	−0·000 (4)	0·000 (4)
	0·027 (2)	0·000 (2)
		0·024 (2)

Direction cosines of the principal axes of the **LST** matrices

$$\mathbf{L}\ (\theta_b = 25°)\begin{pmatrix} 0{\cdot}90628 & 0 & -0{\cdot}42267 \\ 0 & 1 & 0 \\ 0{\cdot}42267 & 0 & 0{\cdot}90628 \end{pmatrix} \qquad \mathbf{S}\ (\theta_a = 45°)\begin{pmatrix} 1 & 0 & 0 \\ 0 & 0{\cdot}70711 & -0{\cdot}70711 \\ 0 & 0{\cdot}70711 & 0{\cdot}70711 \end{pmatrix}$$

$$\mathbf{T}\begin{pmatrix} 1 & 0 & 0 \\ 0 & 1 & 0 \\ 0 & 0 & 1 \end{pmatrix}$$

In Table 6 we give the results of our calculations for the 300 K structure using the following set of charges: +1, +1 and −0·75 for Rb, Zn and Cl ions respectively. This set of charges was found to give a reasonable agreement between the observed (Nakamura, Kasahara & Tatsuzaki, 1980; Rutar, Seliger, Topič & Blinc, 1981) and calculated eigenvalues of Rb(1) and Rb(2) EFG tensors (as the Sternheimer antishielding parameter of Rb is not known we compared not the calculated and observed eigenvalues, but their ratio). In spite of its simplicity, this point-charge model allows for the assignment of the EFG tensors to the corresponding Rb crystallographic sites which cannot be made on the basis of symmetry arguments since, in the paraelectric cell, both Rb atoms lie on a mirror plane perpendicular to the *b* axis. From the results of Table 6, one immediately finds the equivalences:

Rb(1) (our notation) ≡ Rb(II) (Rutar's notation)

and Rb(2) (our notation) ≡ Rb(I) (Rutar's notation).

The calculated orientation of the Rb(1) EFG tensor is in good agreement with the experimental one; although the agreement is much worse for Rb(2) it is reasonably good considering the crudeness of the model (complete neglect of the dipolar contribution of the EFG). Furthermore, in the incommensurate phase the NMR response for this site is a large continuum just below T_i.

The EFG tensors for each Cl ion were calculated with the same set of charges and can be compared with the NQR results of Milia & Rutar (1981). Indeed, for a

Table 6. *Eigenvalues and direction cosines of* ^{87}Rb *EFG tensors in* Rb_2ZnCl_4 *at* 300 K

Ions	λ_i (V/Å⁴)	EFG tensor orientation
(*a*) Calculated from coordinates in Table 2		in *Pnma*, 300 K
Rb(1)	0·012448	$\begin{pmatrix} 0{\cdot}99979 & 0 & -0{\cdot}02027 \\ 0 & 1 & 0 \\ 0{\cdot}02027 & 0 & 0{\cdot}99979 \end{pmatrix} \rightarrow \theta_b \simeq 1°$
	−0·001949	
	−0·010499	
Rb(2)	0·027658	$\begin{pmatrix} 0{\cdot}93077 & 0 & -0{\cdot}36562 \\ 0 & 1 & 0 \\ 0{\cdot}36562 & 0 & 0{\cdot}93077 \end{pmatrix} \rightarrow \theta_b \simeq 21°$
	−0·026725	
	−0·000933	
(*b*) Evaluation from NMR measurements by Rutar which are in good agreement with those of Nakamura		
Rb(I)	$eQ\,V_{ii}/h$, MHz	in *Pcmn*, 308 K
	0·115	$\begin{pmatrix} 0{\cdot}9880 & 0{\cdot}1542 & 0 \\ 0 & 0 & 1 \\ \pm 0{\cdot}1542 & 0{\cdot}9880 & 0 \end{pmatrix} \rightarrow \theta_b \simeq 0°$
	5·365	
	−5·48	
Rb(II)	0·49	$\begin{pmatrix} 0 & \pm 0{\cdot}0214 & 0{\cdot}9998 \\ 1 & 0 & 0 \\ 0 & 0{\cdot}9998 & \pm 0{\cdot}0214 \end{pmatrix} \rightarrow \theta_b \simeq 1°$
	3·27	
	−3·75	

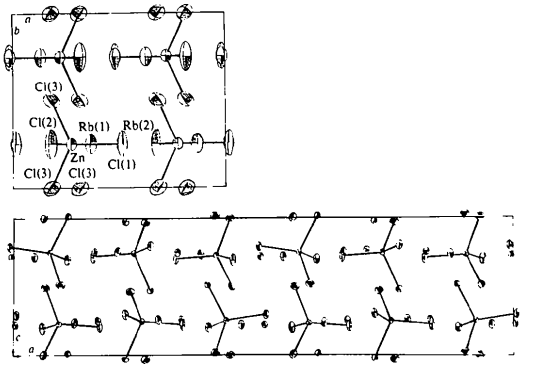

Fig. 1. Projections of the structure at 300 (top) and 100 K (bottom) on one principal plane.

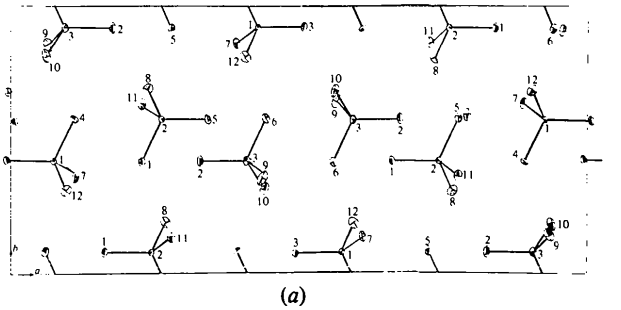

(*a*)

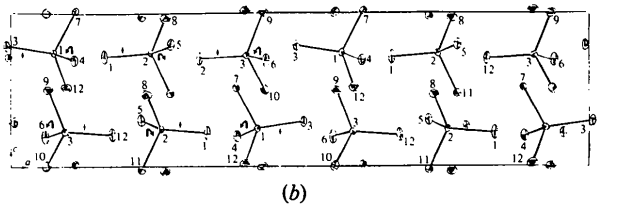

(*b*)

Fig. 2. Projections of the structure at 100 K, on the two principal planes (Rb atoms are omitted). The arrows indicate the displacements of the $ZnCl_4$ groups from their locations in the *Pnma* paraelectric structure.

spin $I = 3/2$ nucleus, the NQR frequency ν_Q can be written as

$$\nu_Q = \frac{e^2 qQ}{h}(1 + \eta^{2/3})^{1/2} = e\frac{Q}{h} V_{zz}(1 + \eta^{2/3})^{1/2}$$

where $e^2 qQ/h$ is the quadrupole coupling constant, η the asymmetry parameter $|V_{xx} - V_{xy}/V_{zz}|$ and V_{il} are the components of the diagonalized EFG tensor using the conventional labelling $|V_{zz}| > |V_{yy}| > |V_{xx}|$. Comparing the experimental frequency (Milia & Rutar, 1981) with the calculated values of $V_{zz}(1 + \eta^{1/3})^{1/2}$ leads to the following assignment

Cl(1) (our notation) ≡ Cl(*d*) (Milia's notation)
Cl(2) ≡ Cl(*c*)
Cl(3) ≡ Cl(*a*, *b*).

We have performed the same calculations with our results obtained at 100 K. Table 7(*a*) gives the EFG tensors of Rb ions. These results can be compared to those presented by Rutar *et al.* (1981). We also calculated the EFG tensors of Cl ions, which allowed us to assign the NQR lines in the ferroelectric phase given in Milia & Rutar (1981) (see Table 7*b*).

Table 7. *Eigenvalues, direction cosines and EFG tensors*

(*a*) Eigenvalues and direction cosines of ^{87}Rb EFG tensors in Rb_2ZnCl_4 at 100 K

Ions	λ_i (V/Å^4)	*Pna*2$_1$, 100 K
Rb(1)	0·01393	(0·86343 −0·13425 0·48628)
	−0·01169	(0·35255 0·85006 −0·39130)
	−0·00224	(−0·36084 0·50930 0·78129)
Rb(2)	0·00938	(0·95541 0·25888 0·14201)
	−0·00236	(−0·29527 0·83669 0·46126)
	−0·00702	(0·00060 −0·48263 0·87582)
Rb(3)	0·01986	(0·83043 0·12766 −0·54230)
	−0·01086	(0·00508 0·97162 0·23650)
	−0·00410	(0·55710 −0·19915 0·80621)
Rb(4)	0·02391	(0·91831 −0·39159 −0·05794)
	0·00129	(0·35690 0·88234 −0·30674)
	−0·02528	(0·17124 0·26100 0·95003)
Rb(5)	0·02728	(0·90876 0·41067 −0·07418)
	−0·00259	(−0·40246 0·90946 0·10446)
	−0·02469	(0·11037 −0·06508 0·99176)
Rb(6)	0·02262	(0·93086 −0·35339 0·09282)
	0·00322	(0·29491 0·87666 0·38012)
	−0·02585	(−0·21571 −0·32646 0·92027)

(*b*) From the Cl EFG tensor calculation, assignments of ν(NQR) proposed by Milia

Reference 10 of Milia, paraelectric	This work, ferroelectric phase	
Cl(*a*)	Cl(7)	Cl(9)
Cl(*b*)	Cl(11)	Cl(5)
	Cl(6)	Cl(8)
Cl(*c*)	Cl(4)	
	Cl(12)	
	Cl(10)	
Cl(*d*)	Cl(13)	
	Cl(12)	
	Cl(1)	

IV. Structural modulation

As we mentioned in § III, refinements in the incommensurate phase give R factors which are rather high and thermal parameters which assume large and unrealistic values.

Two models were used to try to explain the observed data.

(*a*) *Split-atom model*

This model makes use of a classical procedure when dealing with this kind of problem. The structure is refined at 300 and 235 K with this model in which each Cl atom is divided fictitiously into two parts. The average *Pnma* structure is derived from the hexagonal prototype one, by an order–disorder transition associated with a triply-degenerate soft mode. This makes it worthwhile to study the occupancy of each Cl in the average split model. This was done by refining the occupancy of the Cl atoms with a constraint applied satisfying symmetry requirements.

The atomic parameters of the ordered model listed in Table 2 were employed as initial parameters in the least-squares calculation. At 235 K refinement converged to residuals $R = 0{\cdot}063$ and $R_w = 0{\cdot}069$ while the residuals of the ordered model are $R = 0{\cdot}084$ and $R_w = 0{\cdot}109$. The split-atom model for Rb atoms did not lead to significant improvement of the residuals.

At 300 K refinement converged to $R = 0{\cdot}066$ and $R_w = 0{\cdot}070$. For the two temperatures all the Cl atoms show the same occupancy of 0·5.

The final atomic parameters are listed in Tables 8(*a*) and 8(*b*).

Table 8. *Atomic fractional coordinates* (× 10^4) *and thermal parameters* (*see deposition footnote*) *for the split-atom model* (Cl *atoms only*)

Asterisks indicate fixed values. $B_{eq} = \frac{8}{3}\pi^2 \sum_i \sum_j U_{ij} a_i^* a_j^* \mathbf{a}_i . \mathbf{a}_j$.

	x	y	z	B_{eq} (Å^2)
(*a*) *Pna*2$_1$, 300 K				
Rb(1)	6316 (3)	¼*	4073 (3)	2·81 (1)
Rb(2)	4851 (2)	¼*	8195 (2)	1·69 (1)
Zn(1)	2246 (2)	¼*	4223 (2)	1·08 (1)
Cl(1)	9840 (2)	2778 (21)	4174 (2)	2·30 (2)
Cl(2)	3186 (2)	2790 (24)	5855 (1)	2·33 (2)
Cl(3)	3236 (9)	9888 (13)	3565 (7)	2·03 (1)
Cl(4)	3050 (11)	4844 (12)	3250 (7)	2·61 (1)
(*b*) *Pna*2$_1$, 235 K				
Rb(1)	6302 (3)	¼*	4069 (3)	2·33 (1)
Rb(2)	4862 (2)	¼*	8194 (2)	1·37 (1)
Zn(1)	2240 (2)	¼*	4219 (2)	0·82 (1)
Cl(1)	9827 (2)	2824 (12)	4189 (2)	1·80 (2)
Cl(2)	3208 (2)	2867 (9)	5849 (1)	1·88 (2)
Cl(3)	3228 (7)	9857 (9)	3579 (5)	1·68 (1)
Cl(4)	3032 (9)	4804 (10)	3207 (5)	2·30 (1)

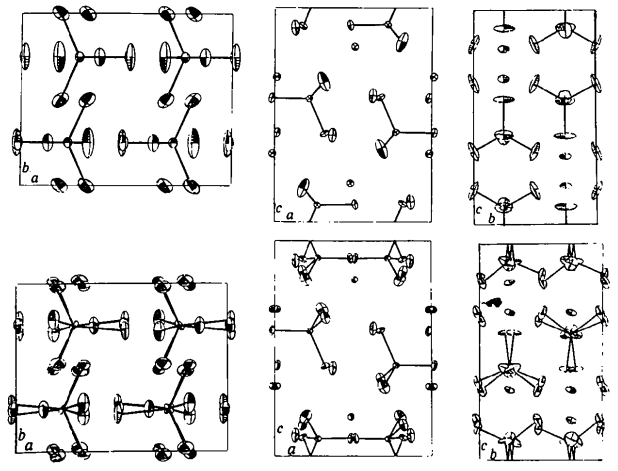

Fig. 3. Projections of the structure at 235 K on the three principal planes using the *Pnma* approximation (top row) and the split-atom model (bottom row).

Fig. 3 shows *ORTEP* projections of the structure on the three principal planes for the ordered and the split models at 235 K.

If we compare the results of the ordered and split models we notice that the atomic positions almost agree between the two models. In the split-atom model the diagonal thermal vibrations are roughly divided by a factor of 2, and the direction connecting the split positions of each atom agrees with the principal direction of the thermal vibration having the largest amplitude in the ordered model.

As we are dealing with an average structure, the improvement we get using the split model is not spectacular, but nevertheless these results do not rule out the existence in the incommensurate phase of a possible disordering of the $ZnCl_4$. This is in agreement with previous experimental results obtained by Raman (Quilichini, Mathieu, Le Postellec & Toupry, 1982), neutron (Currat, Joffrin, Pick & Quilichini, 1980) and NMR spectroscopy (Blinc, Ložar, Rutar & Žumer, 1982).

(*b*) *Triple-cell model*

In this case we fictitiously triple the unit cell and refine in the space group $Pna2_1$ from the independent reflection data obtained at 235 K. Fitting calculations were nearly impossible with all parameters free showing the instability of such a system.

(*c*) *Modulation at* 100 K

From the results of structure refinements we observe that we need two 'parameters' to describe the modulation which triples the unit cell along the pseudo-hexagonal axis on going from the paraelectric space group *Pnma* to the ferroelectric space group $Pna2_1$.

One of the 'parameters' is the rotation of the $ZnCl_4$ group around an axis nearly parallel to **a**. One could say that in the distorted pseudo-hexagonal paraelectric phase (*Pnma*) this $ZnCl_4$ group has three possible orientations and on going to the ordered ferroelectric phase ($Pna2_1$) the orientation of one group corresponds to one of three orientations in the disordered state.

The other 'parameter' is the tilt (up or down **c**) of the shortest Zn–Cl bond parallel to **a**. It is to be noted that the *c* axis of $Pna2_1$ corresponds to the *b* axis of *Pnma* and that the spontaneous polarization of the ferroelectric state is parallel to this axis.

In agreement with previous studies (Quilichini *et al.*, 1982; Currat *et al.*, 1980), it is suggested that a displacive model is not sufficient by itself to account for the successive phase transitions, but, as in $NaNO_2$ (Durand, 1982), one has to deal with an order–disorder model describing the arrangement of the $ZnCl_4$ groups.

V. Possible space group of the low-temperature phase

At 60 K we refined the raw data in the space group $Pna2_1$. The *R* factors are quite satisfactory, but, as mentioned in § III.3, it is certain that the space group $Pna2_1$ is not correct because we detected Bragg peaks which are systematically absent in this group. We carefully went back to the raw data and noticed that all these peaks are very weak which explains why in the preceding attempt with a powder sample (Pannetier & Quilichini, 1980) we did not see them.

Furthermore for such weak reflections the possibility of multiple scattering cannot be excluded. Amongst these lines were selected only about 20 peaks which could be called 'significant' based on the peak–background ratio.

From the Raman study (Francke *et al.*, 1980; Quilichini *et al.*, 1982) and from group-theory analysis Dvorak & Kind, 1981) we think there is at least a doubling of the unit cell at the phase transition T_0. Looking at these reflections we searched for systematically extinct reflections in the space group of phase V (Table 9*a*).

Let us assume that the doubling of the cell is induced by a wavevector $\mathbf{k} = (\mathbf{b}_2 + \mathbf{b}_3)/2$. Working with Kovalev's (1965) notation this leads to the space group $A1a1$ which is in agreement with Dvorak (Dvorak & Kind, 1981). The primitive vectors of the unit cell are $\mathbf{a}_1$, $\mathbf{a}_2 + \mathbf{a}_3$, $\mathbf{a}_2 - \mathbf{a}_3$. The antisymmetrized square of the doubly-degenerate representation which induces the transition does not have the vector representation, so we have a possible second-order antiferrodistortive phase transition. Table 9(*b*) gives the correspondence between the notations of *International Tables for X-ray Crystallography* (1952) and those of Kovalev.

Table 9. *Selected forbidden Bragg peaks observed at 60 K, and correspondence of notations*

(*a*) Example of selected forbidden Bragg peaks observed at 60 K, classified with the conditions of possible reflections in space group $Pna2_1$

hkl	$\lvert F_{obs}\rvert$*	$\sigma(F)$	*hkl*	$\lvert F_{obs}\rvert$*	$\sigma(F)$
*h*00 condition			*h*0*l* condition		
9 0 0	1·43	0·11	1 0 1	0·93	0·11
			3 0 1	1·25	0·09
0*k*0 condition			3 0 2	1·00	0·16
0 1 0	0·46	0·16	3 0 3	1·15	0·22
0 3 0	0·86	0·14	3 0 4	0·81	0·35
			5 0 2	2·40	0·08
00*l* condition			5 0 4	1·21	0·21
0 0 1	0·90	0·11	9 0 2	1·19	0·16
0 0 3	1·5	0·25	9 0 5	1·05	0·30
			11 0 4	1·23	0·32
			13 0 5	1·29	0·30

(*b*) Correspondence between the notations of *International Tables* and Kovalev, for space group $Pna2_1$

International Tables	Kovalev
x, y, z	$\{h_1\}$
$\bar{x}, \bar{y}, \frac{1}{2}+z$	$\left\{h_4 \middle\vert \frac{a_1+a_2+a_3}{2}\right\}$
$\frac{1}{2}-x, \frac{1}{2}+y, \frac{1}{2}+z$	$\left\{h_{25} \middle\vert \frac{a_1+a_2}{2}\right\}$
$\frac{1}{2}+x, \frac{1}{2}-y, z$	$\left\{h_{27} \middle\vert \frac{a_1}{2}\right\}$

* Corrected for absorption.

The conditions for possible reflections in this space group are *h*0*l* with $h = 2n$ and *hkl* with $k + l = 2n$ and have to be rewritten in the $Pna2_1$ frame of reference using the transformation matrix from $Pna2_1$ to $A1a1$.

Starting with the violated conditions given in Table 9(*a*) in $Pna2_1$ we see that 0*k*0, 00*l*, *h*0*l* give $0k\bar{k}$, 0*ll*, *hll* respectively in $A1a1$ and are not in contradiction with the conditions for possible reflections in this space group. Only the *h*00 condition in $Pna2_1$ obtained from the 900 peak leads to a condition which is not compatible with $A1a1$. This 900 peak is unique and very weak and its presence could be explained by multiple scattering.

The other group proposed by Dvorak is $P1a1$, deduced from the space group $Pna2_1$ using $\mathbf{k} = \mathbf{b}_3/2$. The representation which induces the transition is one-dimensional and satisfies the Lifshitz criterion. Working with this space group in the same way as before, we see that it cannot be excluded. As a conclusion, based on previous results (Raman) and the present ones, we can propose the space group $A1a1$ for phase V. Nevertheless, we are aware that we could have started with other assumptions from a strictly crystallographic point of view, and finally to define unambiguously the space group of phase V, a more direct measurement should be made (for example, with Weissenberg neutron equipment).

Note added in proof: During the submission for publication of this work we were informed of an X-ray study of the structure of Rb_2ZnCl_4 at 295 K by Secco & Trotter. Their results are in very good agreement with the structure proposed at 300 K in the present paper.

References

BLINC, A., LOŽAR, B., RUTAR, V. & ŽUMER, S. (1982). *Solid State Commun.* **42**, 679–681.

COOGAN, C. K. (1967). *Aust. J. Chem.* **20**, 2551–2565.

COPPENS, P. & HAMILTON, W. C. (1970). *Acta Cryst.* A**26**, 71–83.

CRUICKSHANK, D. W. J. (1956). *Acta Cryst.* **9**, 757–758.

CURRAT, R., JOFFRIN, C., PICK, R. M. & QUILICHINI, M. (1980). ILL Annual Reports.

DURAND, D. (1982). Thèse de 3e cycle, Univ. of Paris XI.

DVORAK, V. & KIND, R. (1981). *Phys. Status Solidi B*, **107**, K109–K113.

FRANCKE, E., LE POSTOLLEC, M., MATHIEU, J. P. & POULET, H. (1980). *Solid State Commun.* **34**, 183–185.

GÜNTER, P., SANCTUARY, R. & ROHNER, F. (1982). *Phys. Status Solidi A*, **70**, 583–589.

International Tables for X-ray Crystallography (1952). Vol. I. Birmingham: Kynoch Press.

JOHNSON, C. K. (1965). *ORTEP.* Report ORNL-3794. Oak Ridge National Laboratory, Tennessee.

KOESTER, L. & RAUCH, H. (1979). *Summary of Neutron Length.* IAEA Contract 25/7/RB.

KOVALEV, O. H. (1965). *Irreducible Representations of Space Groups.* London: Gordon & Breach.

LEHMANN, M. S. & LARSEN, F. K. (1979). *Acta Cryst.* A**30**, 580–584

MILIA, F. & RUTAR, V. (1981). *Phys. Rev. B*, **23**, 6061–6066.

NAKAMURA, T., KASAHARA, M. & TATSUZAKI, I. (1980). *J. Phys. Soc. Jpn*, **49**, 1429–1433.

PANNETIER, J. & QUILICHINI, M. (1980). ILL Annual Reports.

QUILICHINI, M., MATHIEU, J. P., LE POSTELLEC, M. & TOUPRY, N. (1982). *J. Phys. (Paris)*, **43**, 787–793.

RUTAR, V., SELIGER, J., TOPIČ, B. & BLINC, R. (1981). *Phys. Rev. B*, **24**, 2397–2402.

SECCO, A. S. & TROTTER, J. (1983). *Acta Cryst.* C**39**, 317–318.

SCHOMAKER, V. & TRUEBLOOD, K. N. (1968). *Acta Cryst.* B**24**, 63–76.

SHELDRICK, G. M. (1976). *SHELX.* Program for crystal structure determination. Univ. of Cambridge, England.

UNRUH, H.-G. & STRÖMICH, J. (1981). *Solid State Commun.* **39**, 737–740.